A Fully Automatic Breast Ultrasound Image Segmentation Approach Based On Neutro-Connectedness

Min Xian, H. D. Cheng
Computer Science Department of
Utah State University
Logan, Utah, USA
{min.xian, hd.cheng}@aggiemail.usu.edu

Yingtao Zhang
School of Computer Science of
Harbin Institute of Technology
Harbin, Heilongjiang, China
yingtao@hit.edu.cn

***Abstract*—Breast tumor segmentation is an important step of breast ultrasound (BUS) computer-aided diagnosis (CAD) systems. However, because of the poor quality of BUS images, it's a challenging task to develop a robust and accurate segmentation algorithm. Much progress has been made on applying fuzzy connectedness to segment objects from low quality images. However, the fuzzy connectedness method still has difficulty in segmenting objects with weak boundaries. The neutrosophic set theory has been widely applied to image processing, and shows more strengths in modeling uncertainty and indeterminacy. In this paper, two new concepts of neutrosophic subset and neutrosophic connectedness (*neutro-connectedness*) were defined to generalize the fuzzy subset and fuzzy connectedness. The newly proposed *neutro-connectedness* models the inherent uncertainty and indeterminacy of the spatial topological properties of the image. The proposed method is applied to a breast ultrasound database with 131 cases, and its performance is evaluated by similarity ratio (SIR), false positive ratio (FPR) and average Hausdroff error (AHE). In comparison with the fuzzy connectedness segmentation method, the proposed method is more accurate and robust in segmenting tumors in BUS images.**

***Keywords*—**neutrosophic set; fuzzy connectedness; neutro-connectedness; tumor segmentation

I. INTRODUCTION

Breast cancer is one of the leading causes of cancer death among females worldwide, and breast ultrasound (BUS) is a major imaging mode for early detection of breast cancer. Tumor segmentation is a prerequisite step of BUS computer-aided diagnosis (CAD) systems, and is essential for further quantitative analysis of breast lesions [1-5]. The final result provides accurate location of a lesion and excludes normal tissues. In many early CAD systems, tumors were manually marked by trained radiologists. This operator-dependent tumor segmentation method inevitably introduces subjective bias and results in a great deal of tedious work, which makes it impractical to widely use BUS CAD systems in clinical applications.

To address the above problem, several automatic tumor segmentation methods [1, 2, 4, 5] have been proposed. However, the tumor boundaries in BUS image are typical weak and ambiguous because of the intrinsic uncertainty of BUS imaging. Most of the BUS segmentation methods did not model the inherent uncertainty and indeterminacy of the tumor boundaries in BUS images; therefore, they cannot effectively distinguish the tumor from the normal regions (fat, shadowing artifacts, etc.). Furthermore, many methods were dependent on certain hard and inflexible constraints, such as fixed reference point (RP) for selecting seeds or ROI [1, 4, 6], or region size and spatial location for refining candidate ROIs [5], which impede the application of these methods to BUS CAD systems as well.

An ideal automatic tumor segmentation method should have the following three main characteristics: (1) it is fully automatic; (2) it can handle the weak boundaries, and can effectively distinguish and exclude the normal regions from the tumor region and (3) the constraints based on empirical domain knowledge must be soft in order to achieve high generalization and robustness.

The fuzzy connectedness, modeling the uncertainty of the spatial topological property of the images, has attracted a great attention in image segmentation. But the nature of fuzzy connectedness makes it easy to leak through weak boundaries, and results in high false positive rate.

Neutrosophic logic extended the fuzzy logic and is more powerful than fuzzy methods in dealing with uncertainty and indeterminacy [9]. In this paper, we proposed a fully automatic tumor segmentation approach for BUS images. Two new concepts, neutrosophic subset and neutrosophic connectedness (*neutro-connectedness*), were introduced to solve the weak and ambiguous boundary problem which is a critical issue in image segmentation.

This paper is organized as follows: in section II, the background of neutrosophic set is presented; in section III, the newly proposed neutrosophic subset and *neutro-connectedness* are defined; in section IV, we apply the proposed theory to segment tumors in BUS images automatically; in section V, the experimental results are discussed; and the conclusion is given in section VI.

This work is supported, in part, by National Science Foundation of China; the Grant number is 61100097.

1051-4651/14 $31.00 © 2014 IEEE
DOI 10.1109/ICPR.2014.431

II. NEUTROSOPHIC SET

Neutrosophic logic was developed as an extension of fuzzy logic to handle the indeterminacy better by introducing the indeterminacy set [11]. Neutrosophic set generalizes the fuzzy set, and its properties have been discussed [9, 10, 17].

The classical "problem of reviewers" shows that the neutrosophic method can solve some tasks which cannot be solved by fuzzy methods: two reviewers (A and B) rank a paper with memberships μ_A and μ_B. Assume that $\mu_A = \mu_B$=0.8, and they have different background qualifications. Although they give the same membership, it will have different effects on the paper decision.

In a Neutrosophic set ***S***, three subsets, **<S>**, <**Neut-S**> and <**Anti-S**>, are defined to describe truth, indeterminacy and falsity subsets, respectively [11]. <**Anti-S**> is the opposite of <**S**> and <**Neut-S**> is neither <**S**> nor <**Anti-S**>. For example, if <**S**> is defined as "white" on the colors of the objects, then <**Anti-S**> = "black", and <**Neut-S**> will be the colors except white and black (blue, yellow, red, etc.).

Let **U** be a universe of discourse, and $\mathbf{M} \subset \mathbf{U}$. And three symbols, **T, I, F**, are introduced to represent **<S>**, <**Neut-S**> and <**Anti-S**> respectively. An element ***x*** from **M** is noted with respect to set **M** as ***x***(***t***, ***i***, ***f***) and belongs to **M** in the following way: it is ***t*** true in the set, ***i*** indeterminate (unknown if it is) in the set, and ***f*** false, where ***t***, ***i***, and ***f*** are elements in **T**, **I**, **F**, respectively. For most real world applications, **T**, **I**, $\mathbf{F} \subset [0,1]$; and $t + f = 1$, and $i \in [0,1]$.

III. PROPOSED METHOD

A. Neutrosophic Subset

In order to model the inherent imprecision in images, Rosenfeld [7] proposed the concept of 2D fuzzy subset and related methods on grayscale image. In Ref. [8], L. Chen et al. extended the 2D fuzzy subset to handle the spatial uncertainty in multidimensional range images (e.g., color images) by introducing the concept of fuzzy subfibber and discussing its properties.

A fuzzy subset $\underset{\sim}{S}$ of a universe **U** is defined as $\underset{\sim}{S} = \{(p, \mu(p)) \mid p \in \mathbf{U}\}$, where $\mu(p)$ refers to the degree of membership of element p in $\underset{\sim}{S}$ and $\mu(p) \in [0,1]$. In a gray image, **U** refers to a set includes all pixels' integer coordinates.

An N-dimensional and *n*-range fuzzy subfiber [8] of a universe **U** is defined as:

$$\underset{\sim}{S}^{Nn} = \left\{\left(p^N, \mu^n\left(p^N\right)\right) \mid p^N \in \mathbf{U}\right\} \tag{1}$$

where p^N refers to an *N*-dimensional point, and *n* is the dimension of the membership function representing a mapping from p^N to $[0, 1]^n$. When *N* equals 2 and *n* equals 1, $\underset{\sim}{S}^{Nn}$ will be the Rosenfeld fuzzy subset.

Based on the membership function, the above two methods could model the imprecision of the data; however, both of the papers did not take the indeterminacy into consideration.

Definition 1: Let **U** be a universe of discourse, a neutrosophic subset $\underset{\sim}{S}_u$ is defined as

$$\begin{aligned} &\underset{\sim}{S}_u = \{(p^N, (\mathbf{T}^n(p^N), \mathbf{I}^n(p^N), \mathbf{F}^n(p^N))) \mid p^N \in \mathbf{U}\} \\ &\mathbf{T}^n(p^N), \mathbf{I}^n(p^N), \mathbf{F}^n(p^N) \in [0,1]^n \end{aligned} \tag{2}$$

where element p^N is an arbitrary *N*-dimensional data, and **T, I,** and **F** defines the degree of truth, indeterminacy, and falsity of element p^N in $\underset{\sim}{S}_u$ respectively.

When $\mathbf{I}^n(p^N) = [0]^n, \mathbf{T}^n + \mathbf{F}^n = [1]^n, \forall p^N \in \mathbf{U}, \mathbf{T}^n(p^N) \in [0,1]^n$, the defined neutrosophic subset will become the fuzzy subfiber. And if $\mathbf{I}^n(p^N) = [0]^n, \mathbf{T}^n + \mathbf{F}^n = [1]^n$, $\forall p^N \in \mathbf{U}, \mathbf{T}^n(p^N) \in [0,1]^n$, $N = 2$ and $n = 1$, it will become the fuzzy subset.

B. Neutro-Connectedness

Connectedness of entities is an important topological property in image processing. The fuzzy connectedness defined on fuzzy subset has attracted great attention and has been widely applied to image segmentation [7, 8, 12-14]. However, the fuzzy connectedness did not model the inherent indeterminacy of image properties, which make it difficult to segment objects from low quality images.

In this section, we propose the *neutro-connectedness* based on the 2D neutrosophic subset to deal with the indeterminacy of the connectedness which can overcome the deficiency of fuzzy connectedness.

Definition 2: Let *S* be a set including all pixels' coordinates in an image and Z_i be the *ith* path between two points on *S*. The strength of the *neutro-connectedness* of Z_i is a triple which is defined as

$$\begin{aligned} &NC_{path}(Z_i) = \left(\Pi^T(Z_i), \Pi^I(Z_i), \Pi^F(Z_i)\right) \\ &Z_i = \left(z_1, \ \ldots\ , z_l\right), z_k \in S, k = 1, \cdots, l \end{aligned} \tag{3}$$

where $\Pi^T(Z_i), \Pi^I(Z_i)$ *and* $\Pi^F(Z_i)$ represent the degree of truth, indeterminacy and falsity of the connectedness of path Z_i, respectively. They are defined as follows.

$$\begin{aligned} &\Pi^T(Z_i) = \min\{\mu_\kappa(z_j, z_k) \mid z_k \in \mathbb{N}\left(z_j\right), z_j, z_k \in Z_i\} \\ &\Pi^I(Z_i) = \max\{\mu_\beta(z_j, z_k) \mid z_k \in \mathbb{N}\left(z_j\right), z_j, z_k \in Z_i\} \\ &\Pi^F(Z_i) = 1 - \Pi^T(Z_i) \end{aligned} \tag{4}$$

In Eq. (4), we use $\mathbb{N}(z_j)$ to represent the set of 8-connected neighbors of pixel z_j, μ_κ to represent the strength of connectedness between adjacent points, and μ_β to represent the degree of indeterminacy of the connectedness.

Definition 3: Let $\mathbb{Z}$ be the set of all the paths between pixels p and q in set S. The *neutro-connectedness* between p and q is denoted as $NC(p,q)$ and is defined in Eq. (5).

$$NC(p,q)=\begin{pmatrix} t(p,q)=\Pi^{T}(Z_d)=\max(\Pi^{T}(Z_i)), \\ i(p,q)=\Pi^{I}(Z_d), \quad |Z_i\in\mathbb{Z} \\ f(p,q)=1-\Pi^{T}(Z_d) \end{pmatrix} \quad (5)$$

IV. Fully Automatic Tumor Segmentation

In this section, we demonstrate the application of the proposed theory to segment tumors in BUS images automatically. The flowchart of the proposed approach is shown in Fig. 1.

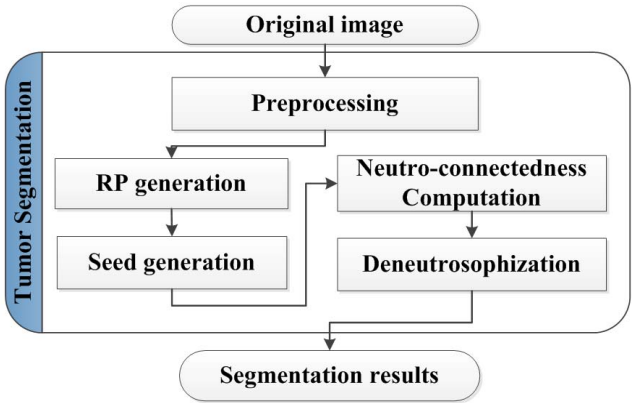

Fig. 1. Flowchart of the proposed method.

A. Fully Automatic Seed Generation

1) Preprocessing

The goal of preprocessing here is to map all intensities into a normalized range, emphasize the low intensities of the tumor region and attenuate intensities of the normal tissues. Let I_0 be the original image, and set S contains all pixels' 2D coordinates. The preprocessing is performed in following steps.

a) Smoothing: A discrete Gaussian low-pass filter was applied to smooth the BUS image in the frequency domain. The filter is defined as

$$H(m,n)=\frac{1}{z}\exp\left(\frac{-d^2(m,n)}{2d_0^2}\right), z=\sum_{m=1}^{M}\sum_{n=1}^{N}H(m,n) \quad (6)$$

where $d(m, n)$ is the distance from position (m, n) to (M/2, N/2), d_0 is the cutoff frequency and M and N are the numbers of rows and columns, respectively. The BUS image I_0 is Fourier transformed, then multiplied with filter H to attenuate high frequencies, and then transformed back to the spatial domain to obtain a smoother image I.

b) Normalization: A Z-shaped function was used to transform the intensities of the smoothed image I into [0, 1].

In Eq. (7), $I(x)$ is the gray value of point x on image I; the parameters a and c locate the limits of the curve's sloped portion and control the nonlinear range of the curve; the parameter b is used to adjust the steepness of the curve which is defined in Eq. (8).

$$Z(I(x);a,b,c)=\begin{cases} 1 & I(x)\le a \\ 1-\dfrac{(I(x)-a)^2}{(c-a)(b-a)} & a\le I(x)\le b \\ \dfrac{(I(x)-c)^2}{(c-a)(c-b)} & b\le I(x)\le c \\ 0 & I(x)\ge c \end{cases} \quad (7)$$

$$b=a+SD\cdot SN \quad (8)$$

where a is set as 20 by experiment, SD is the standard deviation of the image intensities, and S_N is the normalized skewness which is defined as [16]

$$SN=E(X)^3\Big/\left(E(X)\right)^3 \quad (9)$$

After the two steps have been completed, we obtained a normalized image W and $W(x)\in[0,1],\forall x\in S$.

2) Seed generation

The seed refers to a pixel in the tumor region. It was the initial point used to calculate the neutro-connectedness.

In algorithm 1, the reference point (RP) is obtained by using the method proposed in Ref. [15], W is the output of the preprocessing, RPs include the original RP and four generated RPs along four directions ($\pi/4,3\pi/4,5\pi/4,7\pi/4$) with distance 10, and the Mean Shift algorithm [18] was used to locate the local maximum position $c(i)$, i=1,2,⋯,5 iteratively.

Algorithm 1:

inputs: RP, W
outputs: *seed*

extend one RP to 5 RPs;
for $i = 1 : 5$
  initialize the start position P to be $RP(i)$;
  iterate until converge to a candidate position $c(i)$;
  compute the local mean $M(i)$ on W;
end
choose the point with the maximum $M(i)$ as the final seed

B. Neutro-connectedness Computation

In order to apply the proposed *neutro-connectedness* to model the uncertainty and indeterminacy of tumor segmentation problem, the specific forms of μ_κ and μ_β need

to be defined.

Let z_j and $z_k \in S$ be two 8-connected neighbors. We define μ_κ as the same as fuzzy *spel* affinity in [12].

$$\mu_K(z_j, z_k) = w_1 h_1(z_j, z_k) + (1 - w_1) h_2(z_j, z_k)$$
$$h_1(z_j, z_k) = \exp(-1/2 \times [((W(z_j) + W(z_k))/2 - m_1)/s_1]^2) \quad (10)$$
$$h_2(z_j, z_k) = \exp(-1/2 \times [|(W(z_j) - W(z_k)| - m_2)/s_2]^2)$$

In Eq. (10), W(z), $z \in \{z_j, z_k\}$, is the value of pixel in the normalized image; function h_1 computes the degree of difference in appearance between the two adjacent pixels and the object of interest; function h_2 is used to impose the boundary constraint; m_1 and s_1 are the mean and standard deviation of the gray values (W) in the object of interest, respectively; m_2 and s_2 are the mean and standard deviation of gray gradient values in the object of interest, respectively.

The degree of indeterminacy between two adjacent points is defined as

$$\mu_\beta(z_j, z_k) = \max\begin{pmatrix} \exp(-1/2 \times [(W(z_j) - m_{12})/s_{12}]^2), \\ \exp(-1/2 \times [(W(z_k) - m_{12})/s_{12}]^2) \end{pmatrix} \quad (11)$$

where m_{12} and s_{12} define a plane between the intensity distributions of object of interest (tumor region) and the non-object (normal tissues). The indeterminacy of connectedness between z_i and z_j will increase when $W(z_i)$ or $W(z_j)$ is close to m_{12}. For any pair of nonadjacent pixels, μ_κ is set to 0 and μ_β is 1.

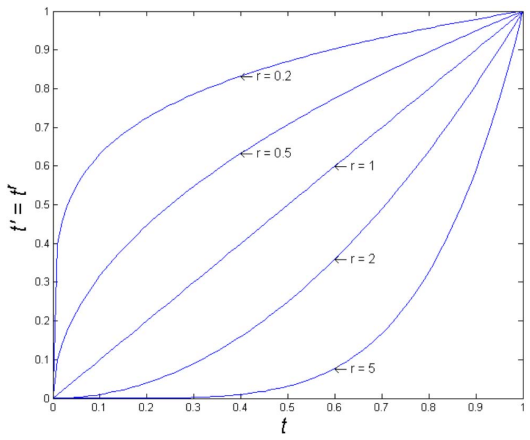

Fig. 2. Domain reduction fuctions

C. De-neutrosophication

We define *de-neutrosophication* to represent the decision making process. In this section, we describe a common strategy used for *de-neutrosophication*. At a high level, the proposed *de-neutrosophication* involves two steps to perform the tumor segmentation:

- Domain reduction. The three domains of the neutro-connectedness (*t*, *i* and *f*) will be reduced into two domains (*t'* and *f'*).
- Graph cuts segmentation. The two domains (*t'* and *f'*) will be applied to constrain the graph cuts to perform the final segmentation.

As shown in Fig. 2, a group of power functions will be employed to do the domain reduction.

In Fig. 2, r is defined as

$$r = \begin{cases} i(p,q), \ if \ \ i(p,q) < 0.5 \\ 1/i(p,q), if \ \ i(p,q) \geq 0.5 \end{cases} \quad (12)$$

where $i(p, q)$ is defined in Eq. (5) . The domain reduction will decrease the connectedness between pixels if the corresponding indeterminacy is bigger than 0.5; otherwise, the connectedness will increase. The f' is set to $1 - t'$.

Graph cuts is chosen to perform the second step of *de-neutrosophication,* and the main reason is that it is easy to integrate different constraints from multi-domains into the segmentation framework in a soft manner [2]. The t' and f' will be used to constrain the global term (data term) of the graph cuts; therefore, the final segmentation will not only consider the local differences and global similarity, but also try to segment the pixels with high connectedness in the same classes (tumor or normal tissues).

If function μ_β is identically equal to 0 ($i(p, q) = 0$, $\forall p, q \in S$), the neutro-connectedness will degenerate into the fuzzy connectedness in Ref. [12]; and λ−connectedness segmentation [8] can be used as the defuzzification to find the final tumor region.

V. Experiment Results

A. Dataset, parameters and metrics

The proposed method was evaluated on a B-mode BUS image database with 131 cases (60 benign and 71 malignant). The radiologist's manually delineated boundaries were used as the golden standards and our segmentation results were evaluated by comparing with them.

The area error metrics and boundary error metrics were employed to evaluate the performance of the proposed segmentation method. The area error metrics include the similarity ratio (*SIR*) and false positive ratio (*FPR*).

$$SIR = |A_m \cap A_r| / |A_m \cup A_r|, FPR = |A_m \cup A_r - A_m| / |A_m|$$

where A_m is the pixel set of the tumor region manually outlined by the radiologist, and A_r is the pixel set of the tumor region generated by the proposed method. The average Hausdorff error (AHE) [6] is used to assess the average performance of boundaries agreement on the database.

The weight w_1 was set to 0.5[12]. The parameters of prior

distribution (m_1, s_1), (m_2, s_2) and (m_{12}, s_{12}) were select as (0.13, 0.2), (0.62, 0.07) and (0.38, 0.2) by experiments, respectively.

B. Results

1) Neutro-connectedness

The *neutro-connectedness* is an extension of the fuzzy connectedness: it not only defines the strength of connectedness between every pair of image pixels, but also gives the indeterminacy of the corresponding connectedness.

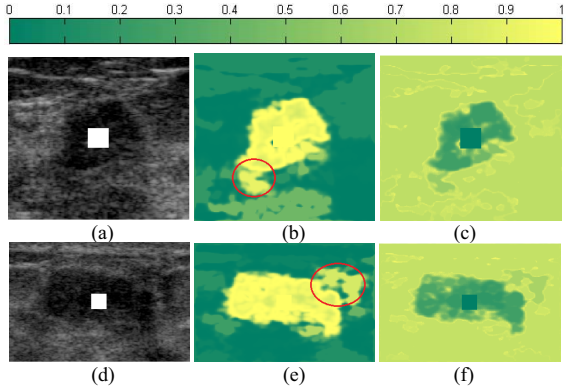

Fig. 3. Calculating connectedness and indeterminacy of two BUS images: (a) and (d) two ROIs (white rectangle) of the original BUS images with weak boundaries, and the white squares are seed regions; (b) and (e) the strength of fuzzy connectedness between each pixel and the seed regions; (c) and (f) the degrees of indeterminacy of the *neutro-connectedness*.

The ROIs are generated automatically from the original BUS images, and the seed regions are small square (side lengths = 21 pixels) regions around the seed points. Fig. 3(a) and (d) are two ROIs generated automatically from the original BUS images. As shown in Fig. (b) and (e), the fuzzy connectedness leaks through the weak parts (red circles) of the boundaries, and links the tumor region with the nearby normal regions. It will produce wrong segmentation results (high false positives). Fig. 3(c) and (f) show the indeterminacies of the neutro-connectedness calculated by using the proposed method. The normal regions with high fuzzy connectedness in Fig. 3(b) and (e) have relatively high indeterminacy in Fig. (c) and (f). It will prevent the leakage of the fuzzy connectedness.

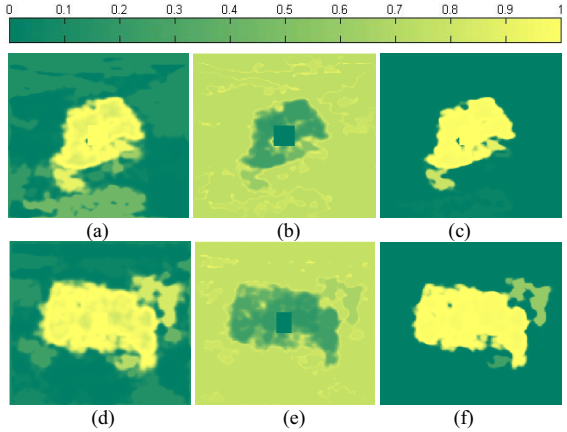

Fig. 4. *De-neutrosophication*: (a) and (d) the fuzzy connectedness of two BUS images (same with Fig. 1(b) and (e)); (b) and (e) the inderminacies (same with Fig. 1(c) and (f)); (c) and (f) the results of domain reductin (*t'*).

2) Domain reduction

In order to apply the *neutro-connectedness* to solve the tumor segmentation problem, we reduced the three domains (*t*, *i* and *f*) into two domains (*t'* and *f'*) using the proposed method. As shown in Fig. 4, the strength of the connectedness between the tumor-like region and tumor is reduced by applying the indeterminacy of connectedness.

3) Segmentation

Based on the same database, we compared our method with the fuzzy connectedness based segmentation method.

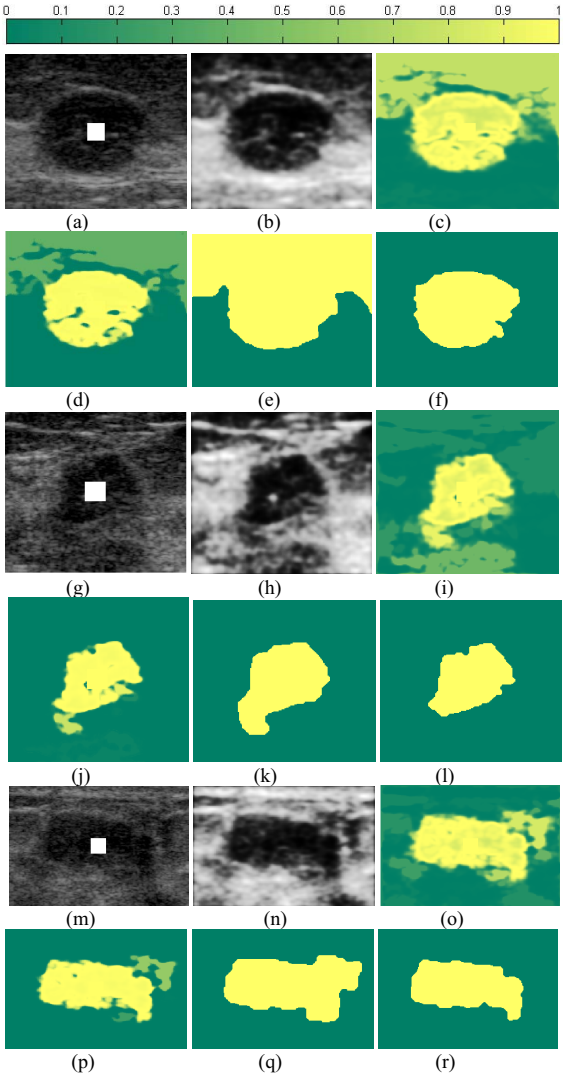

Fig. 5. BUS image segmentation: (a), (g) and (m) three ROIs with seed regions (white rectangle); (b), (h) and (n) the results of the preprocessing step; (c), (i) and (o) the results of fuzzy connectness; (d), (j) and (p) the indeterminacies of the *neutro-connectedness*; (e), (k) and (q) the results of the fuzzy connectedness based segmentation; (f), (l) and (r) the results of the proposed method.

The tumor segmentation of three ROIs of BUS images are shown in Fig 5. Figs. 5(a) – (r) show the intermediated results and the final results of the fuzzy connectedness method and the

proposed *neutro-connectedness* method. As shown in Figs. (c), (i) and (o), the fuzzy connectedness leaks through the weak boundaries and links the tumor regions with the nearby normal regions, which finally results in the increasing of the false positive (Figs. (e), (k) and (g)). Figs. (d), (j) and (p) show that the false connectedness produced by the fuzzy connectedness can be largely reduced by applying the proposed *neutro-connectedness* method, and the results of the proposed method (Figs. (f), (l) and (r)) are much better that of the fuzzy connectedness method.

In order to validate the overall performance of the proposed method, the SIR, FPR and AHE were computed and showed in Table 1. As shown in Table 1, the SIRs of the proposed method on both the benign and the malignant cases are higher than the SIRs of fuzzy connectedness method; which indicates that the results of the proposed segmentation method are more similar to the manually outlined tumor regions than that of the fuzzy connectedness method. The FPRs of the proposed method are much smaller than the FPRs of the fuzzy connectedness method; therefor, the proposed method can exclude most of the tumor-like regions (shadows and fat) from the tumor regions by employing the *neutro-connectedness*. The smaller AHEs also show that the tumor boundaries produced by the proposed method are much closer to the manually outlined boundaries than the boundaries produced by the fuzzy connectedness method.

TABLE I. AVERRAGE PERFORMACE OF TUMOR SEGMENTATION

Cases		Fuzzy connectedness based segmentation			Proposed method		
		SIR (%)	*FPR* (%)	*AHE*	*SIR* (%)	*FPR* (%)	*AHE*
A	60	79.47	**22.30**	20.0	80.92	**6.90**	18.0
B	71	78.48	**23.99**	24.0	82.43	**4.99**	21.6
C	131	78.93	**22.74**	22.2	79.65	**9.85**	20.9

A: benign tumors; B: malignant tumors; C: total.

VI. CONCLUSION

In this paper, the traditional concepts of fuzzy subset and fuzzy connectedness were generalized to the neutrosophic domain, and we proposed two new concepts: the neutrosophic subset and *neutro-connectedness*. Based on the newly proposed theory, a novel tumor segmentation method was proposed to locate the tumors in BUS images. This approach models the spatial topological property of image pixels using the neutro-connectedness to handle the weak boundary problem of BUS images.

The experiments demonstrate that the proposed method is more accurate and robust. The excellent results are guaranteed by following reasons: (1) The newly proposed *neutro-connectedness* can model the indeterminacy resulted from weak boundaries better than fuzzy connectedness; (2) the proposed preprocessing is an effective method to enhance the contrast between the tumor region and the regions of normal tissues; (3) the *neutro-connectedness* constrained graph cuts can find its globally optimal quickly by using the max-flow min-cut algorithm.

REFERENCES

[1] J. Shan, H. D. Cheng, Y. Wang, "Completely automated segmentation approach for breast ultrasound images using multiple-domain features", *Ultrasound in Medicine & Biology*, vol. 35, no. 2, pp. 262-275, 2012.

[2] M. Xian, J. H. Huang, Y. T. Zhang et al. "Multiple-domain knowledge based MRF model for tumor segmentation in breast ultrasound images", In *ICIP*, 2012, pp. 2021-2024..

[3] H. D. Cheng, J. Shan, W. Ju et al., "Automated breast cancer detection and classification using ultrasound images: A survey," *Pattern Recognition*, vol. 43, no. 1, pp. 299-317, 2010.

[4] J. Shan, H. D. Cheng, and Y. Wang, "A novel automatic seed point selection algorithm for breast ultrasound images." In *ICPR*. 2008.

[5] B. Liu, H. D. Cheng, J. Huang et al., "Automated segmentation of ultrasonic breast lesions using statistical texture classification and active contour based on probability distance," *Ultrasound in Medicine & Biology*, vol. 35, no. 8, pp. 1309-1324, 2009.

[6] A. Madabhushi, and D. N. Metaxas, "Combining low-, high-level and empirical domain knowledge for automated segmentation of ultrasonic breast lesions," to *IEEE Trans. Med. Imaging*, vol. 22, no. 2, pp. 155-169, 2003.

[7] A. Rosenfeld, "Fuzzy Digital Topology," *Information and Control,* vol. 40, no. 1, pp. 76-87, 1979.

[8] L. Chen, H. D. Cheng, and J. P. Zhang, "Fuzzy Subfiber and Its Application to Seismic Lithology Classification," *Information Sciences-Applications,* vol. 1, no. 2, pp. 77-95, Mar, 1994.

[9] M. Zhang, L. Zhang, and H. D. Cheng, "A neutrosophic approach to image segmentation based on watershed method," *Signal Processing,* vol. 90, no. 5, pp. 1510-1517, 2010.

[10] H. D. Cheng, Y. Guo, and Y. Zhang, "A Novel Image Segmentation Approach Based On Neutrosophic Set And Improved Fuzzy C-Means Algorithm," *New Mathematics and Natural Computation,* vol. 7, no. 01, pp. 155-171, 2011.

[11] F. Smarandache, *A Unifying Field in Logics: Neutrosophic Logic: Neutrosophy, Neutrosophic Set, Neutrosophic Probability*: American Research Press, 2003.

[12] J. K. Udupa, and S. Samarasekera, "Fuzzy connectedness and object definition: Theory, algorithms, and applications in image segmentation," *Graphical Models and Image Processing,* vol. 58, no. 3, pp. 246-261, 1996.

[13] H. He, and Y. Q. Chen, "Fuzzy aggregated connectedness for image segmentation," *Pattern Recognition,* vol. 34, no. 12, pp. 2565-2568, 2001.

[14] M. Hasanzadeh, and S. Kasaei, "Fuzzy Image Segmentation Using Membership Connectedness," *Eurasip Journal on Advances in Signal Processing*, 2008.

[15] M. Xian, H. D. Cheng, Yingtao Zhang, "Fully Automatic Segmentation of Breast Ultrasound Images Based on Breast Anatomy", submitted to *Pattern Recognition*, 2014.

[16] P. M. Shankar, V. A. Dumane, C. W. Piccoli *et al.*, "Computer-aided classification of breast masses in ultrasonic B-scans using a multiparameter approach," *IEEE Trans. Ultrasonics Ferroelectrics and Frequency Control,* vol. 50, no. 8, pp. 1002-1009, 2003.

[17] Y. Guo, and H. D. Cheng, "New neutrosophic approach to image segmentation," *Pattern Recognition*, vol. 42, no. 5, pp. 587-595, 2009.

[18] Y. Z. Cheng, "Mean Shift, Mode Seeking, and Clustering," *IEEE Trans. Pattern Anal. Mach. Intell.*, vol. 17, no. 8, pp. 790-799, Aug, 1995.